Pannexin 1 mediates ferroptosis that contributes to renal ischemia/reperfusion injury

Received for publication, September 5, 2019, and in revised form, October 22, 2019 Published, Papers in Press, November 6, 2019, DOI 10.1074/jbc.RA119.010949

Lianjiu Su[‡], Xiaofang Jiang[‡], Cheng Yang[‡], Jiahao Zhang[‡], Bo Chen[‡], Yiming Li[‡], Shijie Yao[‡], Qin Xie[‡], Hernando Gomez[§], Raghavan Murugan[§], and Zhiyong Peng[‡§1]

From the [‡]Department of Critical Care Medicine, Zhongnan Hospital of Wuhan University, Wuhan, Hubei Province 430071, China and the [§]Center of Critical Nephrology, Department of Critical Care Medicine, University of Pittsburgh Medical Center, Pittsburgh, Pennsylvania 15223

Edited by Qi-Qun Tang

Renal ischemia/reperfusion injury (IRI) is a significant challenge in perioperative medicine and is related to oxidative programmed cell death. However, the role of ferroptosis, a newly discovered form of oxidative cell death, has not been evaluated widely. Pannexin 1 (PANX1), an ATP-releasing pathway family protein, has pro-apoptotic effects during kidney injury. Here, we demonstrate that PANX1 deletion protects against renal IRI by regulating ferroptotic cell death. *Panx1* knockout mice subjected to renal IRI had decreased plasma creatinine, malondialdehyde (MDA) levels in kidney tissues, and tubular cell death (visible as decreased TUNEL-positive renal tubular cells) compared with WT mice. In cultured human kidney 2 (HK-2) cells, silenced *Panx1* expression significantly attenuated ferroptotic lipid peroxidation and iron accumulation induced by the ferroptosis inducer erastin. Moreover, the *Panx1* silencing significantly modulated ferroptosis-related protein expression. Furthermore, *Panx1* deletion induced the expression of a cytoprotective chaperone, heme oxygenase-1 (HO-1), and inhibited ferroptinophagy via the mitogen-activated protein kinase (MAPK)/extracellular signal–regulated kinase (ERK) pathway. In summary, *Panx1* deletion protects against renal IRI by attenuating MAPK/ERK activation in a ferroptotic pathway. Our findings provide critical insights into the role of PANX1 in ferroptotic cell death and highlight a potential therapeutic target for the management of acute kidney injury (AKI) during the perioperative period.

Acute kidney injury (AKI)[2] is a frequent complication after cardiac surgery, which contributes to increased mortality, and has been related to ischemia/reperfusion injury (IRI) (1). Oxidative damage has been widely studied in IRI-AKI, and most current studies focus on harm mediated by apoptosis, autophagy, and necrosis (2–4). Ferroptosis, a newly discovered form of programmed, nonapoptotic cell death triggered by oxidative damage, has not been widely investigated in IRI-AKI. Ferroptosis is an iron-dependent type of programmed cell death, triggered by lipid peroxide accumulation in the context of increased reactive oxygen species (ROS) generation and inactivation of GSH peroxidase 4 (GPX4), a GSH-dependent enzyme that prevents lipid peroxidation (5). It can be triggered by structurally diverse small molecules (*e.g.* erastin, sulfasalazine, and RSL3) and also prevented by lipophilic antioxidants (CoQ10, vitamin E, ferrostatins, and liproxstatins) (6–9). Many regulators such as GPX4, nuclear factor erythroid 2–related factor 2 (Nrf2), heme oxygenase-1 (HO-1), nuclear receptor coactivator 4 (NCOA4), and ferritin light chain 1 (FTH1) have been identified as being involved in regulating ferroptosis (10–13). Ferroptosis has been shown to occur IRI-AKI (14). Furthermore, IRI-AKI has been shown to be attenuated after treatment with the ferroptosis-specific inhibitor ferrostatin-1 (Fer-1) (14). In addition, the augmenter of liver regeneration (ALR) has been shown to prevent IRI-AKI by limiting ferroptosis through the regulation of the GSH-GSH peroxidase (GSH-GPx) system.

Pannexin belongs to the ATP-releasing pathway family and is expressed in almost all cell types. The pannexin family consists of three proteins, Panx1, Panx2, and Panx3, all of which form membrane channels. Among them, Panx1 has been extensively investigated (15, 16). Panx1 is involved in regulating ATP release as a damage-associated molecular pattern (DAMP) molecule that can activate apoptosis or autophagy signaling in oxidative condition (17, 18). ATP binds to the P2Y7 receptor, thereby activating protein kinase C (PKC) and mitogen-activated protein kinase (MAPK) signaling (19), which regulates ferroptosis in Parkinson's disease (20). Importantly, a reduction in this ATP release–dependent signaling has been shown to protect kidneys from oxidative damage during IRI-AKI (21). Therefore, we hypothesized that panx1 deletion protects against IRI-AKI by limiting ferroptosis-mediated oxidative damage. Here, we demonstrate for the first time a role of panx1 in ameliorating ferroptosis in the kidney. Our findings provide new insights to understand the

This work was supported by National Natural Science Foundation of China Grant 81560131 (to Z. P.) and Hubei Province Key Projects Grant WJ2017Z008 (to Z. P.). The authors declare that they have no conflicts of interest with the contents of this article.

[1] To whom correspondence should be addressed: Zhongnan Hospital of Wuhan University, Hubei 430000, China. Fax: 86-27-6781-2892; E-mail: pengzy5@hotmail.com.

[2] The abbreviations used are: AKI, acute kidney injury; IRI, ischemia/reperfusion injury; I/R, ischemia/reperfusion; ROS, reactive oxygen species; GPX4, GSH peroxidase 4; NRF2, nuclear factor erythroid 2–related factor 2; HO-1, heme oxygenase-1; NCOA4, nuclear receptor coactivator 4; FTH1, ferritin light chain 1; DAMP, damage-associated molecular pattern; MAPK, mitogen-activated protein kinase; ERK, extracellular signal–regulated kinase; TUNEL, terminal deoxynucleotidyltransferase-mediated dUTP nick end labeling; JNK, c-Jun N-terminal kinase; ZnPP, zinc protoporphyrin-9; AMPK, AMP-activated protein kinase; MEK, mitogen-activated protein kinase/extracellular signal–regulated kinase kinase; H&E, hematoxylin and eosin; 7-AAD, 7-aminoactinomycin D; Scr, serum creatinine.

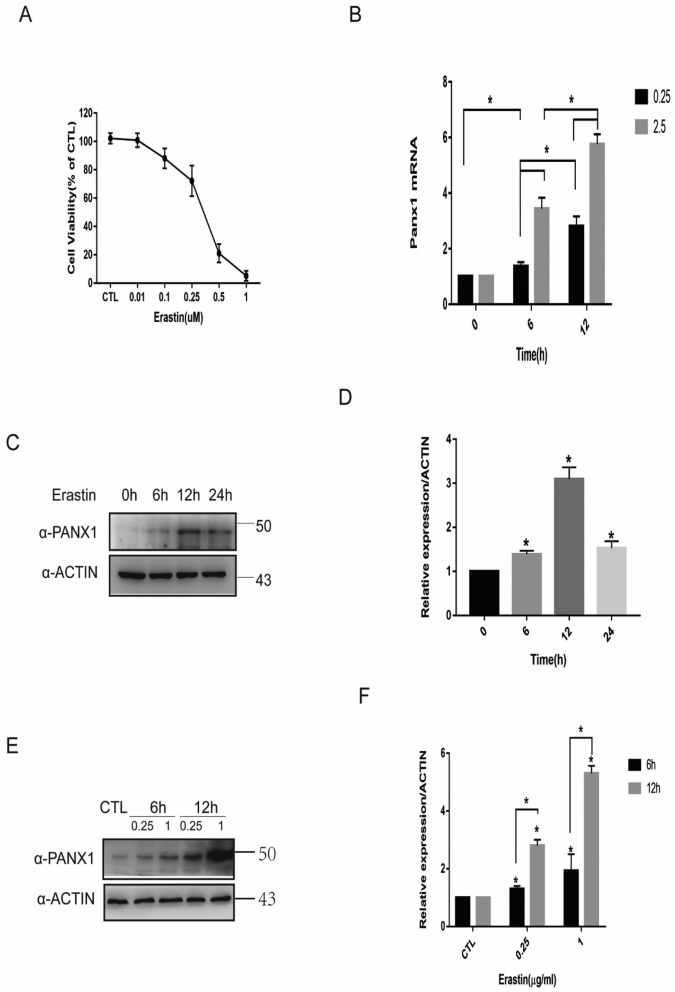

Figure 1. Increased Panx1 expression during erastin-induced ferroptosis in HK-2 cells. *A*, HK-2 cells treated with erastin in different concentrations for 24 h were subjected to a cell viability test. *B*, HK-2 cells treated with erastin at the indicated concentrations and time intervals for testing mRNA expression by quantitative PCR *versus* control. *C*, a Western blotting assay was utilized to detect Panx1 expression at different time points. *D*, relative expression of *gray values* for *C* ($n = 3$, mean ± S.D. (*error bars*); *, $p < 0.05$). *E*, HK-2 cells treated with erastin at the indicated concentrations and time intervals for testing protein expression by Western blot analysis. *F*, relative expression of *gray values* for *E* ($n = 3$, mean ± S.D.; *, $p < 0.05$).

mechanism of panx1 in ferroptotic cell death and highlight a new therapeutic target for AKI treatment.

Results

Panx1-regulated erastin-induced ferroptosis in human kidney-2 (HK-2) cells

Increased Panx1 expression levels of HK-2 upon erastin—As a special ferroptosis inducer, erastin has been widely studied in ferroptosis for abolishing the import of cysteine, a precursor for GSH during ferroptosis (22–24). We performed a CCK-8 assay to investigate erastin-mediated cell death in HK-2 cells and found a significantly decreased cell viability at an erastin concentration of 0.1 μg/ml (Fig. 1*A*). To examine whether the induction of ferroptosis by erastin regulates panx1 expression, we next analyzed protein and mRNA expression levels of panx1 in HK-2 cells. Remarkably, treatment with erastin significantly induced panx1 mRNA (Fig. 1*B*) and protein expression in a time- and concentration-dependent manner (Fig. 1, *C*, *D*, *E*, and *F*).

Panx1 silencing inhibits erastin-induced ferroptosis in HK-2 cells and decreases lipid peroxidation, iron accumulation, and mitochondrial membrane potential hyperpolarization—To investigate whether up-regulated panx1 confers to ferroptosis induced by erastin, we first measured cell viability after panx1 pharmacologic inhibition or knockdown using a specific shRNA. Similar to results from previous studies (6), several ferroptosis inhibitors (ferrostatin-1 and DFO) significantly reversed erastin-induced cell death (Fig. 2*A*). Three sequences of shRNA were designed and testing by quantitative PCR (Fig. 2*B*), and Western blotting was used to verify the most efficient sequence (Fig. 2*C*). Suppression of panx1 expression both genetically and pharmacologically, significantly inhibited erastin-induced ferroptotic cell death in HK-2 cells (Fig. 2, *A* and *D*). Examination of the morphology of cells using an inverted microscope and cell death analysis by flow cytometry showed that panx1 knockdown significantly inhibited erastin-induced ferroptotic cell death in HK-2 cells (Fig. 2, *E–G*). To characterize cell death by erastin, we measured key characteristics of ferroptosis in HK-2 cells, including lipid peroxidation and labile iron levels (6). Lipid ROS were measured using the dye C11-BODIPY 581/591, and labile iron levels were significantly increased following treatment with erastin. In contrast, panx1 knockdown decreased lipid peroxidation and iron accumulation (Fig. 2, *H–J*). Mitochondria play a pivotal role in ferroptosis, and its membrane potential hyperpolarization is associated with ferroptotic cell death (25). As the results shown that panx1 knockdown decreased mitochondrial membrane potential hyperpolarization (Fig. 2*K*).

Panx1 regulates the expression of ferroptosis-related proteins in HK-2—Previous studies have shown that proteins involved in iron and ROS metabolism, such as NCOA4, NRF2, HO-1, and FTH1, play a role in ferroptosis (10, 12, 13). Therefore, we analyzed the expression of proteins translated by NCOA4, NRF2, HO-1, FTH1, and GPX4. In response to erastin, NCOA4 and FTH1 expression increased at the first 6 hour and then declined (Fig. 3, *A* and *B*). The expression of NRF2 and HO-1 increased significantly throughout the entire 24-h period, whereas GPX4 expression decreased at 12 and 24 h (Fig. 3, *A* and *B*). To further investigate the role of panx1 in regulating ferroptosis, we exposed panx1 knockdown HK-2 cells to erastin. The expression of NCOA4 and FTH1 was inhibited in HK-2 panx1 knockdown cells in response to erastin (Fig. 3, *C* and *D*). However, panx1 knockdown had no effect on regulating GPX4 and NRF2 expression. In addition, we found that HO-1 expression was significantly up-regulated in panx1 knockdown cells in response to erastin, suggesting that the protective effect of knocking down panx1 may be related to up-regulation of antioxidant genes (Fig. 3, *C* and *D*). Collectively, these findings suggest that panx1 could regulate ferroptosis-related gene involved in iron and ROS metabolism.

Panx1 regulates ferroptosis in ischemia/reperfusion kidney injury

Increased Panx1 expression levels during IRI-AKI—To determine whether Panx1 participates in kidney IRI, we quantified the expression of panx1 in WT mice subjected to kidney IRI. Com-

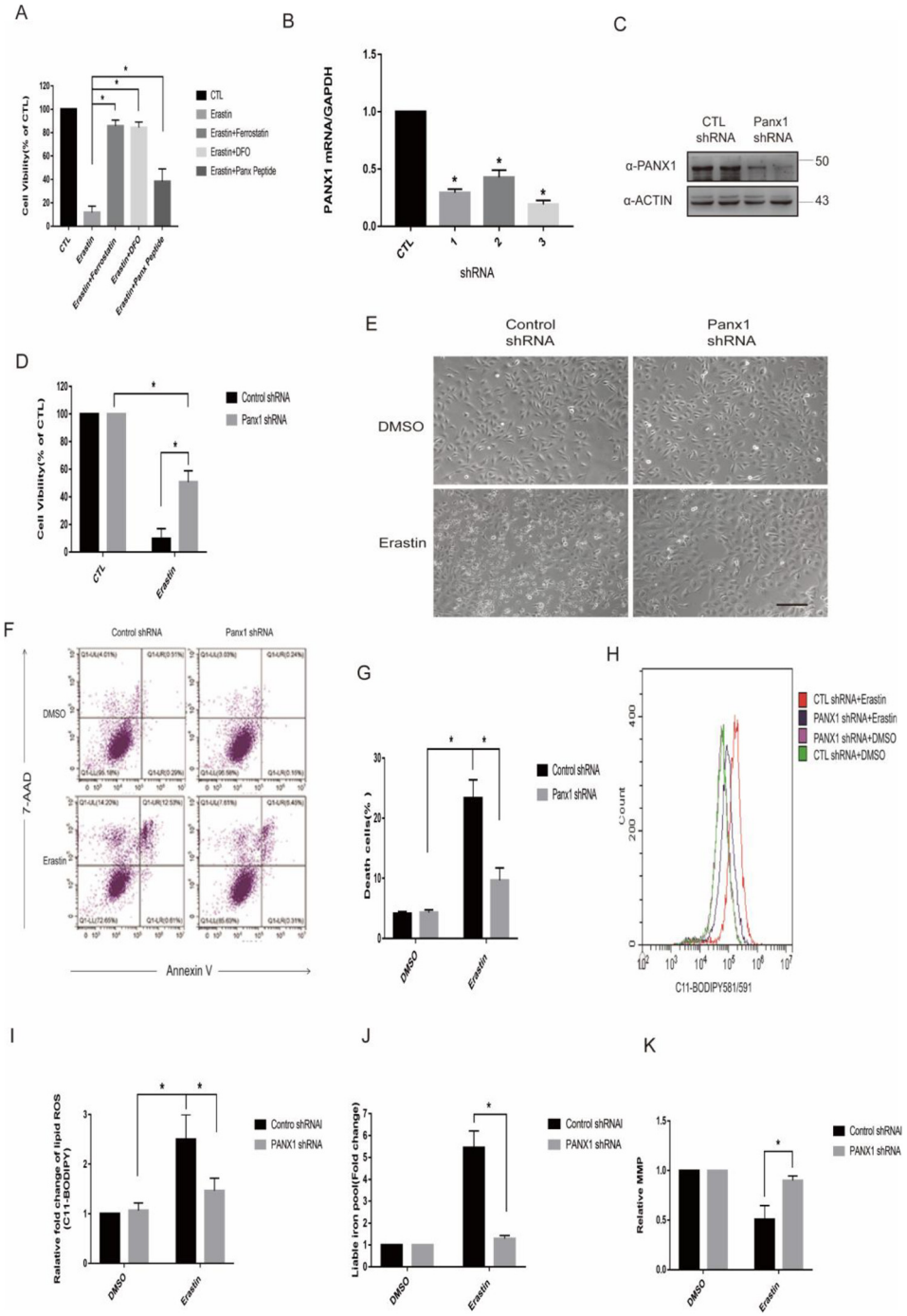

Figure 2. Panx1 knockdown inhibits erastin-induced ferroptosis in HK-2 cells. *A*, HK-2 cells treated with erastin (0.25 μg/ml), ferroptosis inhibitor of ferrostatin (5 μM), DFO (100 μM), and Panx1-specific inhibitor of Panx peptide (10 μM) for 24 h were subjected to a cell viability test. *B*, different shRNA sequences of Panx1 were tested by quantitative PCR *versus* control. *C*, One-third of Panx1 was chosen according to quantitative PCR with the most effective knockdown function and confirmed by Western blotting with two separate transfection experiments. *D*, the indicated knockdown HK-2 cells were treated with erastin (0.25 μg/ml) for 24 h, and cell viabilities were assayed ($n = 3$; *, $p < 0.05$). *E*, the indicated knockdown HK-2 cells were treated with erastin (0.25 μg/ml) for 24 h, and cell morphology was observed with an inverted microscope. *Scale bar*, 20 μm. *F*, the indicated knockdown HK-2 cells were treated with erastin (0.25 μg/ml) for 18 h. For annexin V/7-AAD staining, cells were collected, and the proportion of 7-AAD–positive cells (dead) was determined by flow cytometry. *G*, data shown are from three independent experiments of *F* compared with the control (mean ± S.E. (*error bars*); *, $p < 0.05$). *H*, the indicated knockdown HK-2 cells were treated with erastin (0.25 μg/ml) for 18 h and loaded with BODIPY 581/591 for lipid ROS generation analysis. The fluorescent signal was detected by flow cytometry. *I*, data shown from three independent experiments of *H* compared with the control (mean ± S.E.; *, $p < 0.05$). *J*, the indicated knockdown HK-2 cells were treated with erastin (0.25 μg/ml) for 24 h, and labile iron levels were assayed ($n = 3$; *, $p < 0.05$). *K*, the indicated knockdown HK-2 cells were treated with erastin (0.25 μg/ml) for 18 h and loaded with JC-1 for mitochondrial membrane potential.

pared with sham mice, both mRNA and protein expression of Panx1 were up-regulated significantly at 6 and 12 h after IRI, suggesting that IRI induces Panx1 renal expression (Fig. 4, *A–D*).

Panx1 deletion prevents kidney injury induced by ischemia/reperfusion—The effect of Panx1 gene deletion in kidney was confirmed by Western blotting and immunohistochemis-

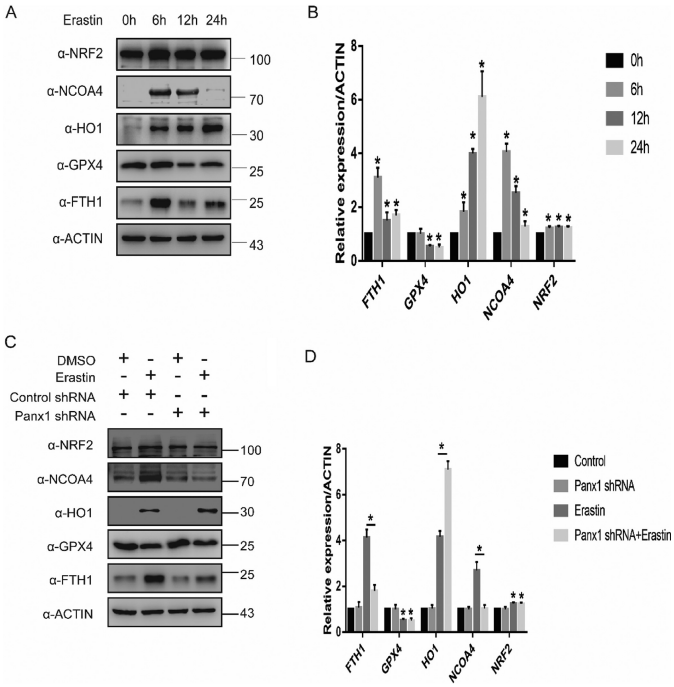

Figure 3. Panx1 regulates the expression of ferroptosis-related protein in HK-2. *A*, ferroptosis-related protein expression at different time points was assayed using Western blotting. *B*, relative expression of *gray values* for *A* ($n = 3$, mean ± S.D. (*error bars*); *, $p < 0.05$). *C*, Panx1 knockdown–regulated ferroptosis-related protein expression tested by Western blotting. *D*, relative expression of *gray values* for *C* ($n = 3$, mean ± S.D.; *, $p < 0.05$).

try (Fig. 5, *A* and *B*). To confirm the role of panx1 in kidney IRI, we compared markers of renal injury in WT *versus* panx1 knockout mice subjected to I/R. We assessed kidney function by measuring serum creatinine and investigating histological features. Serum creatinine (Scr) and tissue damage were similar between WT and panx1 knockout mice subjected to sham operation (Fig. 5*C*). Scr 24 h after IRI was lower in Panx1 knockout mice than in WT mice (Fig. 5*C*). Consistent with the Scr data, Panx1 knockout mice had decreased renal tubular necrosis, congestion, and cast formation with significantly lower renal injury scores compared with WT mice subjected to renal IRI. (Fig. 5, *D* and *E*). Terminal deoxynucleotidyl transferase–mediated dUTP nick-end labeling (TUNEL) showed increased renal cell death in WT mice when compared with Panx1 knockouts (Fig. 5, *F* and *G*). Tissue lipid peroxidation assessed using MDA levels decreased in Panx1 knockout mice compared with WT (Fig. 5*H*). Taken together, these results suggested that Panx1 deletion prevents kidney injury after ischemia/reperfusion.

Panx1 regulates the expression of ferroptosis-related protein in renal IRI—Previous studies have proven the occurrence of ferroptosis in kidney injury induced by ischemia/reperfusion (11, 14). In our study, we found that ferroptosis-related proteins were up-regulated significantly during IRI (Fig. 6, *A* and *B*). In addition, Panx1 knockout mice had a significant increase in HO-1 expression compared with WT mice after IRI. The expression of ferroptosis-related protein was similar to *in vitro* results (Fig. 6, *C* and *D*).

Panx1 regulates ferroptosis via MAPK/ERK signaling pathway

Previous studies have shown that ATP, as signal transduction molecules, could activate the MAPK pathway in the process of cell proliferation and cell death (26, 27). We hypothesized that panx1 down-regulates the activity of MAPK signaling in HK-2 cells by regulating ATP release, which, in turn, can inhibit ferroptosis. The results showed that panx1 deletion significantly attenuated phosphorylation of ERK expression exposed to erastin but had almost no effect on phosphorylation of p38 and JNK levels (Fig. 6, *E* and *F*). These results indicate that panx1 regulates the activity of MAPK/ERK signaling in HK-2 cells and leads to ferroptosis. We hypothesized that the panx1 channel releases ATP under oxidative stress conditions, and then ATP bound to P2X7R to activate MAPK pathway, resulting in ferroptotic cell death. To test our hypothesis, we conducted ERK inhibitor (LY3214996, 10 μM) and P2Y7 inhibitor (A-740003, 10 μM) to HK-2 cells exposed to erastin. The result shows that inhibiting the P2Y7 receptor significantly decreased phosphorylation of ERK. Inhibiting ERK significantly decreased NCOA4 expression and increased HO-1 expression in the HK-2 cells exposed to erastin (Fig. 6, *G* and *H*). Both of the two inhibitors decreased GPX4 expression, suggesting that the phosphorylation of ERK has two types of effect, and the antioxidant effect of GPX4 may be relatively weak (Fig. 6, *G* and *H*). Treatment of zinc protoporphyrin-9 (ZnPP), a specific inhibitor of HO-1, had no marked effects on ERK levels, suggesting a MAPK/ERK-HO-1 hierarchy as a response to erastin induction (Fig. 6, *I* and *J*). Taking these together, the protective effect of panx1 knockdown in ferroptosis is via activation of the MAPK/ERK pathway to inhibit NCOA4-mediated ferroptinophagy and increase antioxidant gene HO-1 expression.

Discussion

Ferroptosis is a novel type of programmed cell death characterized by iron-dependent increase in ROS, which is known to play crucial roles in cellular proliferation, senescence, and differentiation (22). The most important finding of this study is the identification of an important role of Panx1 in regulating ferroptosis in the kidney, whereby the absence of the panx1 channel protects renal tubular epithelial cells from erastin-induced ferroptosis and kidney injury for IRI.

Pannexin channels are known to play pathological roles in oxidative stress, inflammation, and cell death (28). Previous studies have reported that P2Y7R, a receptor of panx1, triggered cell death that can be reversed by inhibition of ferroptosis production of NADPH oxidase–generated ROS, which suggests a role of panx1 in ferroptosis (29, 30). A decreasing level of GSH leads to lipid peroxidation, which can be tested by a lipophilic fluorescent dye (C11-BODIPY 581/591) *in vitro* (31). Indeed, the present study showed that panx1 knockdown decreases lipid peroxidation in HK-2 exposed to erastin. Iron participates in several biologic functions, including ferroptosis. For instance, increased ROS causes lipid peroxidation and triggers ferroptosis, which can be suppressed using deferoxamine, an iron chelator (9). In addition, higher levels of iron transport proteins increase iron-mediated ROS production, leading to

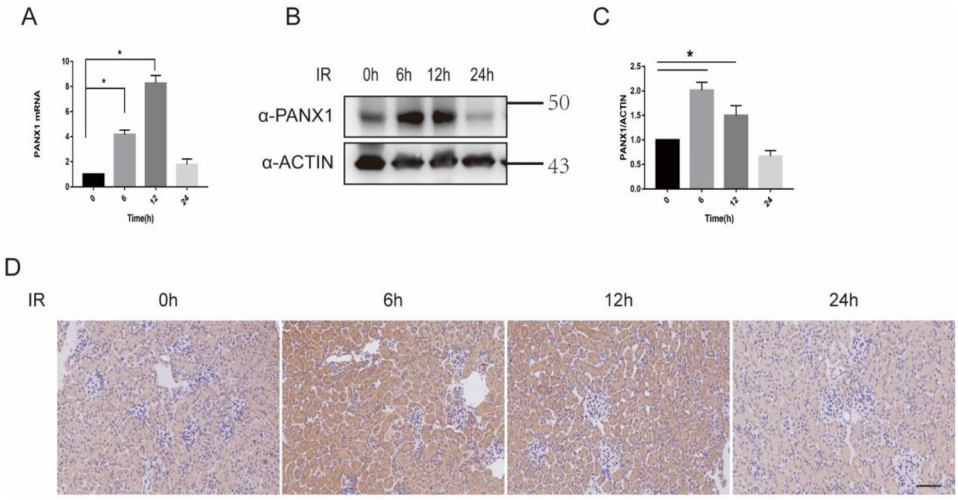

Figure 4. Increased Panx1 expression levels during IRI AKI. *A*, mRNA expression of Panx1 during IRI at different time points assayed by quantitative PCR ($n = 3$; *, $p < 0.05$). *B*, protein levels of Panx1 were assayed using Western blotting ($n = 3$; *, $p < 0.05$). *C*, relative expression of *gray values* for *B* ($n = 3$, mean ± S.D. (*error bars*); *, $p < 0.05$). *D*, protein levels of Panx1 were assayed using immunohistochemistry. *Bar*, 50 μm.

increased ferroptosis (32, 33). In this study, it was observed that iron metabolism–related proteins, such as NCOA4 and FTH1, which maintain cellular labile iron contents, promote the accumulation of cellular ROS and ferroptotic cell death via the "ferroptinophagy" pathway (13, 34). Importantly, panx1 knockdown reduced iron accumulation and reduced iron regulatory gene expression after exposure to erastin, suggesting that panx1 regulates ferroptosis by decreasing cellular iron level. Previous studies have reported that renal proximal tubular cells have limited biosynthetic capacity for GSH *in vitro* and GSH metabolism may not be a requirement for iron-dependent lipid peroxidation (35, 36). Blocking system Xct inhibits cysteine-dependent glutathione (GSH) synthesis and also inhibits the transplasma membrane cysteine redox shuttle (37, 38). Both effects impair cellular antioxidant defenses, thereby facilitating mitochondrial metabolism disfunction and toxic ROS accumulation (6). In regard to erastin-induced HK-2 cell death, it might be due to abolishing the transplasma membrane cysteine redox shuttle, leading to mitochondrial disfunction. The role of mitochondria has been proven to be a motivator in ferroptosis (25, 39). Our results show that panx1 knockdown decreased mitochondrial membrane potential hyperpolarization, suggesting that the protect effect of panx1 deletion in erastin-induced ferroptotic cell death might be due to defending mitochondria disfunction caused by system Xct blocking.

A previous study has investigated the role of ferroptosis in the pathogenesis of IRI-mediated kidney injury (14). In the present study, we have shown that the Panx1 channels in the pathophysiologic pathway of ferroptosis-mediated IRI-AKI, because IRI increases the expression of the Panx1 channel, and knocking out the channel decreases renal injury. Our data suggested that the absence of the Panx1 channel might protect kidney from IRI by limiting lipid peroxidation. We further demonstrated that panx1 deletion further protected the kidney by ameliorating ferroptosis, not through up-regulation of antioxidant genes like GPX4 (40) or Nrf2 (10), but by up-regulating HO-1 expression, which is known to protect against ferroptosis (12, 41). Furthermore, panx1 deletion decreased ferroptosis-related proteins like NCOA4 and FTH1, otherwise up-regulated with IRI. These results illustrated that panx1 could reduce lipid peroxidation to alleviate kidney injury under oxidative stress *in vivo*. We further investigated some ferroptosis-related protein during ischemia reperfusion in panx1$^{-/-}$ mice. GPX4 can neutralize lipid peroxides and protect membrane fluidity by using GSH, as a cofactor of GPX4, to protect cells and membranes against peroxidation (40). NRF2 is responsible for regulating hundreds of antioxidant genes and has been identified as a ferroptosis regulator (10). Our results shown that panx1 deletion has no effect on its expression, suggesting that panx1 could be a gene downstream from them. The cellular defensive response of HO-1 against oxidative stress has been proven to play an important role in ferroptosis (12, 41). In our study, we found that the protective effect of panx1 deletion on ferroptosis was through up-regulation of HO-1 expression. NCOA4 and FTH1, an iron-regulatory protein, regulate ferroptosis in a selective autophagy pathway, so-called "ferritinophagy," which degrades FTH1 to release free iron (42). The results were consistent with an experiment *in vitro* and indicated that panx1 deletion protects the kidney from oxidative damage during IRI by decreasing ferroptosis through modulation of cellular iron levels.

Panx1 was also involved in regulating ATP release, which can activate apoptosis or autophagy signaling (17, 18). Extracellular ATP can act as a paracrine molecule to activate P2X7R, which can regulate various signaling pathways, such as the AMPK and MAPK signaling pathway (43). Previous studies have shown that ferroptosis could activate the MAPK pathway through MEK (20). Our data suggest that the panx1 channel releases ATP under oxidative stress conditions, and then ATP combines with P2X7R to activate the MAPK pathway, resulting in ferroptotic cell death (Fig. 7). We investigated the signal pathway of MAPK regulating ferroptosis. The results demonstrate that panx1 deletion markedly inactivates the MAPK/ERK pathway. The presence of panx1 can inhibit HO-1 expression by activating the MAPK/ERK pathway. Taken together, our data suggest that panx1 deletion

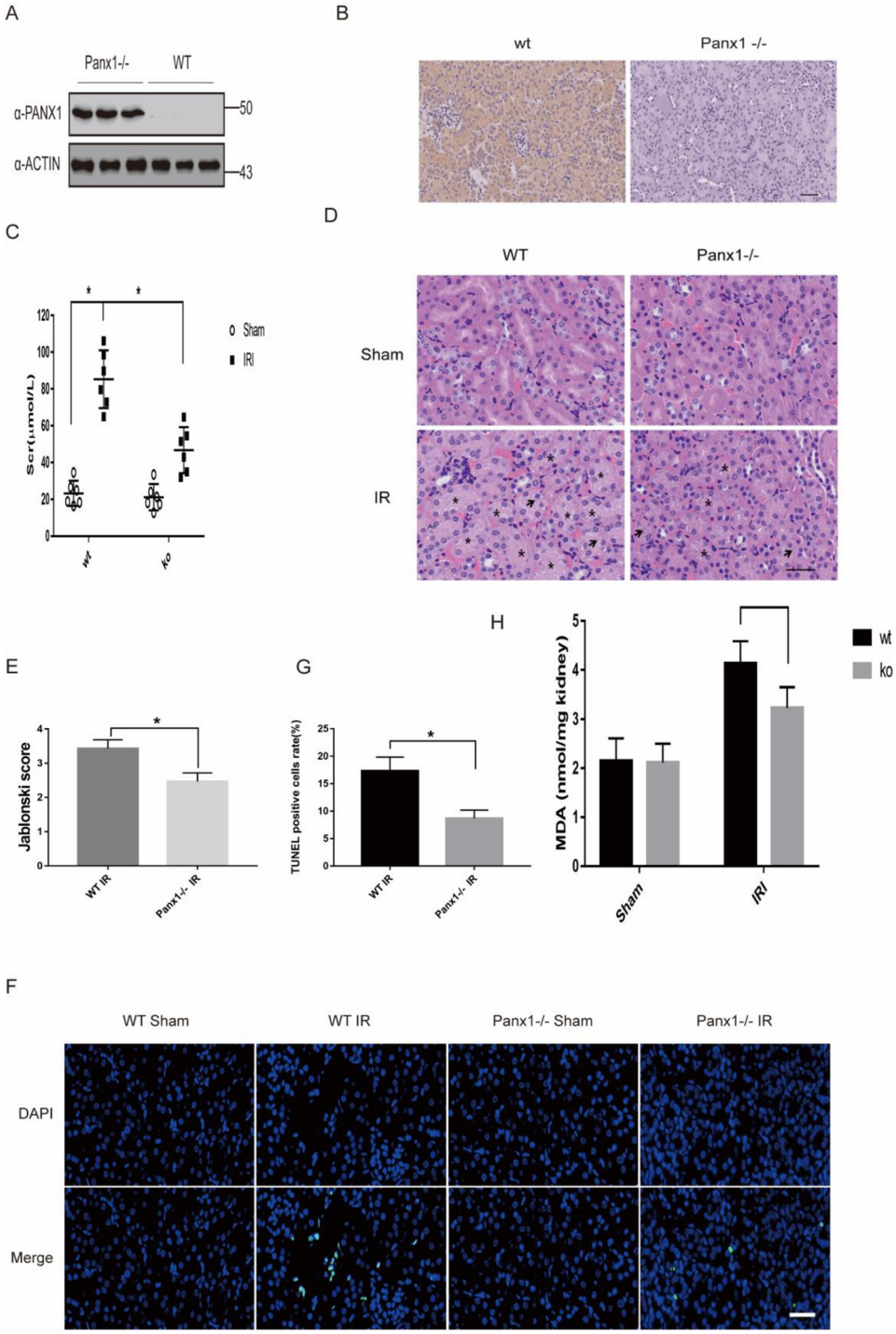

Figure 5. Panx1 deletion prevents kidney injury induced by I/R. *A*, Panx1 knockout mice were confirmed by the protein expression in kidney using Western blotting with three mice *versus* WT. *B*, Panx1 knockout mice were confirmed by the protein expression in kidney using immunohistochemistry. *C*, mice were subjected to sham operation or to 30-min renal ischemia and 24-h reperfusion. Serum creatinine was tested by a kit ($n = 6$; *, $p < 0.05$). *D*, H&E images of mice subjected to 30-min renal ischemia and 24-h reperfusion. *Scale bars*, 20 μm. *E*, the Jablonski scale renal injury score (scale: 0–4) for histology grading was used to grade renal tubular necrosis ($n = 3$; *, $p < 0.05$). *F*, cell death was analyzed by TUNEL in kidneys of mice. *Scale bars*, 20 μm. *G*, TUNEL-positive renal tubular cells were collected from three independent experiments of *F* ($n = 3$; *, $p < 0.05$). *H*, lipid peroxidation in kidney was assessed by MDA level ($n = 6$; *, $p < 0.05$). *Error bars*, S.E.

contributes to modulate the activation of MAPK/ERK and HO-1 signaling pathways, resulting in the inhibition of ferroptotic cell death during IRI.

The unique properties of GSH equilibrium in renal proximal tubular cells *in vitro* (35) may be due to the inactivation of system Xct during erastin-induced HK-2 cell death. GSH synthesis during ferroptosis *in vivo* may be involved. Although we have established that whole-organism Panx1 knockout is protective against IRI, it is unclear whether this mechanism is specific to the kidney. A conditional, renal-specific knockout panx1 would help to further dissect these mechanisms specifically in IRI-AKI. Also, whether Panx1

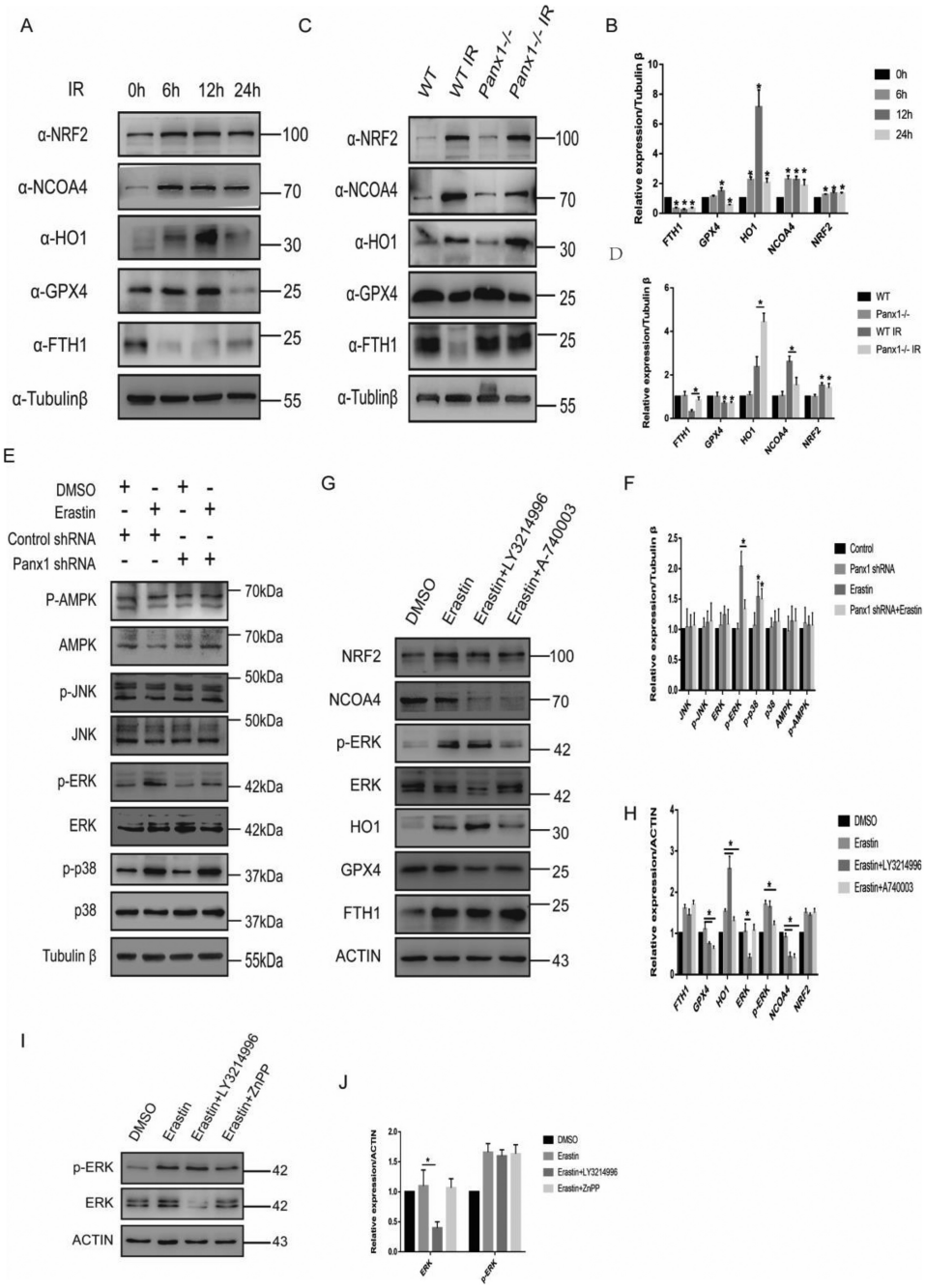

Figure 6. Panx1 regulates ferroptosis in IRI and mediates alternative activation via MAPK/ERK and HO-1 pathway in HK-2. *A*, a Western blotting assay was utilized to detect ferroptosis-related protein expression in IRI mouse kidneys. *B*, relative expression of *gray values* for *A* ($n = 3$, mean ± S.D. (*error bars*); *, $p < 0.05$). *C*, Western blot analysis of ferroptosis-related protein expression in Panx1 knockout and WT mice subjected to IRI or not. *D*, relative expression of *gray values* for *C* ($n = 3$, mean ± S.D.; *, $p < 0.05$). *E*, the indicated knockdown HK-2 cells were treated with erastin (0.25 μg/ml) for 24 h. Shown is Western blot analysis of AMPK, p-AMPK, p38, p-p38, ERK, p-ERK, JNK, and p-JNK protein expression. *F*, relative expression of *gray values* for *E* ($n = 3$, mean ± S.D.; *, $p < 0.05$). *G*, Western blot analysis of ferroptosis-related protein expression in HK-2 cells exposed to erastin (0.25 μg/ml) with ERK inhibitor (LY3214996, 10 μM) or P2Y7 inhibitor (A-740003, 10 μM). *H*, relative expression of *gray values* for *G* ($n = 3$, mean ± S.D.; *, $p < 0.05$). *I*, Western blot analysis of the ERK pathway in HK-2 cells exposed to erastin (0.25 μg/ml) with ERK inhibitor (LY3214996, 10 μM) or HO-1 inhibitor (ZnPP, 5 μM). *J*, relative expression of *gray values* for *I* ($n = 3$, mean ± S.D.; *, $p < 0.05$).

inhibition could protect from other models of AKI (*e.g.* nephrotoxins, obstruction, and sepsis) requires further investigation. Nevertheless, our data suggest that Panx1 inhibition could be a novel therapeutic strategy to attenuate AKI. Further studies are needed to explore safe and effective Panx1-selective inhibitors for therapy in patients with AKI.

In summary, we have shown the role of the Panx1 channel in the regulation ferroptosis in the kidney in response to IRI. Released ATP from the panx1 channel may act as a DAMP that activates ferroptosis via MAPK/ERK signaling and regulates NCOA4-mediated ferroptinophagy and antioxidant gene HO-1 expression (Fig. 7). Therefore, Panx1 inhibition may be a promising therapeutic target to ameliorate AKI in IRI.

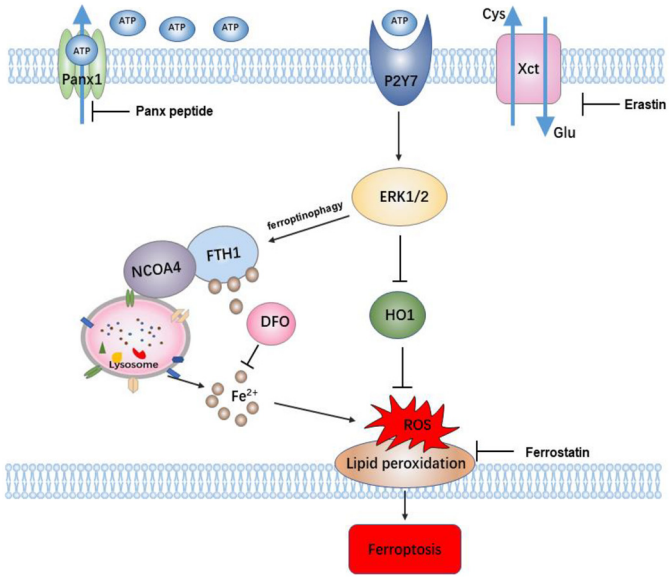

Figure 7. *Schematic* of proposed mechanisms for panx1 regulating ferroptosis in renal IR injury. When HK-2 cells are exposed to ischemia or hypoxia, the Panx1 channel on the membrane opens up and releases ATP. Extracellular ATP as a paracrine molecule combines with P2Y7 receptors to activate the MAPK/ERK signaling pathway, which regulates NCOA4-mediated ferroptinophagy and antioxidant gene HO-1 expression.

Materials and methods

Antibodies and reagents

The antibodies to NRF2 (#ab62352), Panx1 (#ab139715), GPX4 (#ab125066), and NCOA4 (#ab86707) were obtained from Abcam (Cambridge, MA). The antibodies to Panx1 (#91137), actin (#3700), glyceraldehyde 3-phosphate dehydrogenase (#5174), and β-tubulin (#2146) were purchased from Cell Signaling Technology (Danvers, MA). The antibodies to NRF2 (#19693), ERK1/2 (#16443), JNK (#66210), JNK (#614064), and HO-1 (#27282) were taken from Proteintech (Rosemont, IL). The antibodies to p-p38 (#AF4001), p-JNK (#AF3318), and p-ERK (#AF1015) were obtained from Affinity Biosciences (Cincinnati, OH). The antibodies to FTH1 (#sc-28359) and NCOA4 (#sc-373739) were purchased from Santa Cruz Biotechnology, Inc. Deferoxamine (#D9533) and Panx peptide (#SML2082) were taken from Sigma. Erastin (#E7781) and ferrostatin-1 (#S7243) were obtained from Selleck Chemicals (Houston, TX). ZnPP (#B6431) was obtained from APExBIO (Houston, TX).

Cell culture

HK-2 cells were purchased from the Cell Bank of the Chinese Academy of Sciences. The cells were cultured in minimum essential medium (HyClone) with 5 ng/ml human recombinant epidermal growth factor (Novus), 10% fetal bovine serum (Gibco), and a penicillin-streptomycin supplement. The cells were maintained in a humidified incubator at 37 °C and 5% CO_2.

Cell viability assay and cell death analysis

Cell viability was evaluated using a Cell Counting Kit 8 (Dojindo Molecular Technologies, Kumamoto, Japan) assay. Cells were cultured in 96-well plates and treated with the specified compounds for the indicated times. The plates were incubated for an additional 2 h at 37 °C. The absorbance at 450 nm was measured with a microplate reader (ELX-800, BioTek, Winooski, VT). Cell death analysis of ferroptosis followed the method described by Chen *et al.* (46). After treatments, cells were collected and stained with Annexin V-FITC reagent (BioVision) and 7-AAD (Cayman) and subjected to flow cytometry. The percentages of dead cells were quantified with CellQuest software.

Lipid peroxidation, labile iron pool, and mitochondrial membrane potential detection

A special fluorescent dye, BODIPY 581/591 (Thermo Fisher Scientific) is for testing lipid peroxidation *in vitro*. BODIPY 581/591 (1 mM) was incubated for 10 min at 37 °C. The cells were washed with PBS three times, and the intracellular fluorescence was measured by flow cytometry. Evaluating lipid peroxidation *in vivo* used the TBARS method to test MDA level. The total cellular labile iron pool was detected based on the calcein-acetoxymethyl ester method (44). The cells were washed twice with PBS, followed by incubation of 0.05 μM calcein-acetoxymethyl ester (Enzo) for 15 min at 37 °C. Then the cells were washed with PBS and incubated with or without deferiprone (100 μM) for 1 h at 37 °C. After trypsinization, the cells were collected and analyzed by flow cytometry. The levels of the labile iron pool were calculated by the difference in cellular mean fluorescence with and without deferiprone incubation. Mitochondrial membrane potential measurement was done using a JC-1 kit according to the manufacturer's instructions (J8030, Solarbio). Cells were treated as indicated, and then 10 μg/ml JC-1 was added and incubated for 30 min. Labeled cells were trypsinized and resuspended in PBS plus 2% fetal bovine serum. Fluorescence was analyzed using a flow cytometer.

shRNA and transfection protocol

Human Panx1-shRNA (sequence: sense (5′-3′), GCAGCUGCUCCUCAUAUUUTT; sense (3′-5′), AAUGAUGAGUGUCAGCAGGTT) plasmids were purchased from GenePharma (Shanghai, China). Cancer cells were infected with specific shRNA virus–containing supernatant in the presence of Polybrene (8 μg/ml). After 24 h of incubation at 37 °C, the medium was replaced with complete medium containing puromycin (2 μg/ml). The cells were prepared for tests and harvested based on the experiments that were required.

Animal and kidney IRI model

$Panx1^{+/-}$ mice were purchased from GemPharmatech Co., Ltd. (Nanjing, China). $Panx1^{+/-}$ were then mated to C57BL/6 mice, yielding $Panx1^{-/-}$ mice. IRI surgery was performed to induce AKI as described previously (20). Briefly, C57BL/6 mice (male, 10–15 weeks old) were food-deprived for 12 h before the procedures and were anesthetized with intraperitoneal injection of 1% sodium pentobarbital solution (40 mg/kg). Using a midline abdominal incision, bilateral renal IRI was induced by clamping renal pedicles for 30 min. After removal of the clamp, the kidneys were inspected to confirm reperfusion. Body temperature was maintained at 37 °C throughout the procedure. As a control, sham-operated mice underwent the same procedure except for clamping of the renal pedicles. Heparinized blood was centrifuged at 2,000 rpm for 10 min to separate the plasma to detect serum creatinine. The concentration of creatinine in

serum was measured using commercial kit reagents (Institute of Jiancheng Bioengineering, Nanjing, China). The absorbance at 546 nm was detected by a multimode plate reader (PerkinElmer Life Sciences). For tissue analyses, kidneys were harvested, and one half of the harvested kidneys was fixed in 4% paraformaldehyde and processed for H&E staining analysis. The Jablonski renal injury score (scale: 0–4) for histology grading was used to grade renal tubular necrosis 24 h after renal IR. All experiments were performed in accordance with Chinese legislation on the use and care of laboratory animals and were approved by the Animal Care and Use Committee of Wuhan University.

Western blot analysis and quantitative RT-PCR

Total protein was extracted from HK-2 cells and mice kidney tissues. Equal amounts of proteins were separated by SDS-PAGE and transferred to a nitrocellulose membrane (Millipore). After blocking with 5% nonfat milk, the membrane was incubated with specific antibody. All Western blotting analyses were repeated three times. Total RNA was extracted from HK-2 cells, macrophage, and kidney tissues by the YPH EASY spin tissue/cell RNA quick extraction kit (YPH, Beijing, China). In addition, mRNA RT was performed with the ReverTra Ace kit (Toyobo, Osaka, Japan). The cDNA then served as the template for SYBR real-time PCR. Primer sequences were as follows (5′–3′): human panx1 primer sense (5′-CCACCGAGCCCAAGTTCAA-3′) and antisense (5′-GGAGAAGCAGCTTATCTGGGT-3′); mouse Panx1 primer, sense (5′-GCAATACTACACGGAGGAGCACTTC-3′) and antisense (5′-CACCACCCACTGTTCGCTG-3′). All reactions were run in triplicate on the Real-Time PCR Detection System (Bio-Rad).

Immunohistochemistry and TUNEL assay

Immunofluorescence and immunohistochemistry staining were carried out as described previously (45). Panx1 antibody (1:100; Abcam) was used. The sections were visualized using a laser-scanning confocal microscope (FluoView™ FV1000, Olympus, Tokyo, Japan).For the detection of TUNEL-positive cells, the ApopTag Peroxidase In Situ Apoptosis Detection Kit was used according to the manufacturer's instructions (S7100, Serologicals, Millipore).

Statistical analysis

All data are presented as mean ± S.D. unless stated otherwise. Data were analyzed using Student's *t* test for comparison between two groups. $p < 0.05$ was considered statistically significant for all experiments. Statistical analysis was performed using GraphPad Prism 5.0 software.

Author contributions—L. S., C. Y., and B. C. data curation; L. S., J. Z., Y. L., and S. Y. investigation; L. S., X. J., C. Y., J. Z., and Y. L. methodology; L. S. writing-original draft; X. J., S. Y., and Q. X. software; H. G., R. M., and Z. P. writing-review and editing; Z. P. supervision; Z. P. funding acquisition; Z. P. project administration.

References

1. Su, L. J., Li, Y. M., Kellum, J. A., and Peng, Z. Y. (2018) Predictive value of cell cycle arrest biomarkers for cardiac surgery-associated acute kidney injury: a meta-analysis. *Br. J. Anaesth.* **121,** 350–357 CrossRef Medline
2. Meng, X. M., Ren, G. L., Gao, L., Yang, Q., Li, H. D., Wu, W. F., Huang, C., Zhang, L., Lv, X. W., and Li, J. (2018) NADPH oxidase 4 promotes cisplatin-induced acute kidney injury via ROS-mediated programmed cell death and inflammation. *Lab. Invest.* **98,** 63–78 CrossRef Medline
3. Gentle, M. E., Shi, S., Daehn, I., Zhang, T., Qi, H., Yu, L., D'Agati, V. D., Schlondorff, D. O., and Bottinger, E. P. (2013) Epithelial cell TGFβ signaling induces acute tubular injury and interstitial inflammation. *J. Am. Soc. Nephrol.* **24,** 787–799 CrossRef Medline
4. Gu, X., Peng, C. Y., Lin, S. Y., Qin, Z. Y., Liang, J. L., Chen, H. J., Hou, C. X., Wang, R., Du, Y. Q., Jin, J. L., and Yang, Z. J. (2019) P16(INK4a) played a critical role in exacerbating acute tubular necrosis in acute kidney injury. *Am. J. Transl. Res.* **11,** 3850–3861 Medline
5. Stockwell, B. R., Friedmann Angeli, J. P., Bayir, H., Bush, A. I., Conrad, M., Dixon, S. J., Fulda, S., Gascón, S., Hatzios, S. K., Kagan, V. E., Noel, K., Jiang, X., Linkermann, A., Murphy, M. E., Overholtzer, M., *et al.* (2017) Ferroptosis: a regulated cell death nexus linking metabolism, redox biology, and disease. *Cell* **171,** 273–285 CrossRef Medline
6. Dixon, S. J., Lemberg, K. M., Lamprecht, M. R., Skouta, R., Zaitsev, E. M., Gleason, C. E., Patel, D. N., Bauer, A. J., Cantley, A. M., Yang, W. S., Morrison, B., 3rd, Stockwell, B. R. (2012) Ferroptosis: an iron-dependent form of nonapoptotic cell death. *Cell* **149,** 1060–1072 CrossRef Medline
7. Conrad, M., Kagan, V. E., Bayir, H., Pagnussat, G. C., Head, B., Traber, M. G., and Stockwell, B. R. (2018) Regulation of lipid peroxidation and ferroptosis in diverse species. *Genes Dev.* **32,** 602–619 CrossRef Medline
8. Kagan, V. E., Mao, G., Qu, F., Angeli, J. P., Doll, S., Croix, C. S., Dar, H. H., Liu, B., Tyurin, V. A., Ritov, V. B., Kapralov, A. A., Amoscato, A. A., Jiang, J., Anthonymuthu, T., Mohammadyani, D., *et al.* (2017) Oxidized arachidonic and adrenic PEs navigate cells to ferroptosis. *Nat. Chem. Biol.* **13,** 81–90 CrossRef Medline
9. Doll, S., and Conrad, M. (2017) Iron and ferroptosis: a still ill-defined liaison. *IUBMB Life* **69,** 423–434 CrossRef Medline
10. Abdalkader, M., Lampinen, R., Kanninen, K. M., Malm, T. M., and Liddell, J. R. (2018) Targeting Nrf2 to suppress ferroptosis and mitochondrial dysfunction in neurodegeneration. *Front. Neurosci.* **12,** 466 CrossRef Medline
11. Friedmann Angeli, J. P., Schneider, M., Proneth, B., Tyurina, Y. Y., Tyurin, V. A., Hammond, V. J., Herbach, N., Aichler, M., Walch, A., Eggenhofer, E., Basavarajappa, D., Rådmark, O., Kobayashi, S., Seibt, T., Beck, H., *et al.* (2014) Inactivation of the ferroptosis regulator Gpx4 triggers acute renal failure in mice. *Nat. Cell Biol.* **16,** 1180–1191 CrossRef Medline
12. Chang, L. C., Chiang, S. K., Chen, S. E., Yu, Y. L., Chou, R. H., and Chang, W. C. (2018) Heme oxygenase-1 mediates BAY 11-7085 induced ferroptosis. *Cancer Lett.* **416,** 124–137 CrossRef Medline
13. Gao, M., Monian, P., Pan, Q., Zhang, W., Xiang, J., and Jiang, X. (2016) Ferroptosis is an autophagic cell death process. *Cell Res.* **26,** 1021–1032 CrossRef Medline
14. Linkermann, A., Skouta, R., Himmerkus, N., Mulay, S. R., Dewitz, C., De Zen, F., Prokai, A., Zuchtriegel, G., Krombach, F., Welz, P. S., Weinlich, R., Vanden Berghe, T., Vandenabeele, P., Pasparakis, M., Bleich, M., *et al.* (2014) Synchronized renal tubular cell death involves ferroptosis. *Proc. Natl. Acad. Sci. U.S.A.* **111,** 16836–16841 CrossRef Medline
15. Makarenkova, H. P., Shah, S. B., and Shestopalov, V. I. (2018) The two faces of pannexins: new roles in inflammation and repair. *J. Inflamm. Res.* **11,** 273–288 CrossRef Medline
16. Sang, Q., Zhang, Z., Shi, J., Sun, X., Li, B., Yan, Z., Xue, S., Ai, A., Lyu, Q., Li, W., Zhang, J., Wu, L., Mao, X., Chen, B., Mu, J., *et al.* (2019) A pannexin 1 channelopathy causes human oocyte death. *Sci. Transl. Med.* **11,** eaav8731 CrossRef Medline
17. Linden, J., Koch-Nolte, F., and Dahl, G. (2019) Purine release, metabolism, and signaling in the inflammatory response. *Annu. Rev. Immunol.* **37,** 325–347 CrossRef Medline
18. Sun, M., Hao, T., Li, X., Qu, A., Xu, L., Hao, C., Xu, C., and Kuang, H. (2018) Direct observation of selective autophagy induction in cells and tissues by self-assembled chiral nanodevice. *Nat. Commun.* **9,** 4494 CrossRef Medline
19. Xu, J., Chen, L., and Li, L. (2018) Pannexin hemichannels: a novel promising therapy target for oxidative stress related diseases. *J. Cell. Physiol.* **233,** 2075–2090 CrossRef Medline

20. Do Van, B., Gouel, F., Jonneaux, A., Timmerman, K., Gelé, P., Pétrault, M., Bastide, M., Laloux, C., Moreau, C., Bordet, R., Devos, D., and Devedjian, J. C. (2016) Ferroptosis, a newly characterized form of cell death in Parkinson's disease that is regulated by PKC. *Neurobiol. Dis.* **94,** 169–178 CrossRef Medline
21. Jankowski, J., Perry, H. M., Medina, C. B., Huang, L., Yao, J., Bajwa, A., Lorenz, U. M., Rosin, D. L., Ravichandran, K. S., Isakson, B. E., and Okusa, M. D. (2018) Epithelial and endothelial pannexin1 channels mediate AKI. *J. Am. Soc. Nephrol.* **29,** 1887–1899 CrossRef Medline
22. Yang, W. S., and Stockwell, B. R. (2016) Ferroptosis: death by lipid peroxidation. *Trends Cell Biol.* **26,** 165–176 CrossRef Medline
23. Wang, L., Liu, Y., Du, T., Yang, H., Lei, L., Guo, M., Ding, H. F., Zhang, J., Wang, H., Chen, X., and Yan, C. (2019) ATF3 promotes erastin-induced ferroptosis by suppressing system Xc. *Cell Death Differ.* 10.1038/s41418–019-0380-z CrossRef Medline
24. Sun, Y., Zheng, Y., Wang, C., and Liu, Y. (2018) Glutathione depletion induces ferroptosis, autophagy, and premature cell senescence in retinal pigment epithelial cells. *Cell Death Dis.* **9,** 753 CrossRef Medline
25. Gao, M., Yi, J., Zhu, J., Minikes, A. M., Monian, P., Thompson, C. B., and Jiang, X. (2019) Role of mitochondria in ferroptosis. *Mol. Cell* **73,** 354–363.e3 CrossRef Medline
26. Wang, Y., Hall, L. M., Kujawa, M., Li, H., Zhang, X., O'Meara, M., Ichinose, T., and Wang, J. M. (2019) Methylglyoxal triggers human aortic endothelial cell dysfunction via modulation of the KATP/MAPK pathway. *Am. J. Physiol. Cell Physiol.* **317,** C68–C81 CrossRef Medline
27. Su, X., Shen, Z., Yang, Q., Sui, F., Pu, J., Ma, J., Ma, S., Yao, D., Ji, M., and Hou, P. (2019) Vitamin C kills thyroid cancer cells through ROS-dependent inhibition of MAPK/ERK and PI3K/AKT pathways via distinct mechanisms. *Theranostics* **9,** 4461–4473 CrossRef Medline
28. Bond, S. R., and Naus, C. C. (2014) The pannexins: past and present. *Front. Physiol.* **5,** 58 CrossRef Medline
29. Draganov, D., Gopalakrishna-Pillai, S., Chen, Y. R., Zuckerman, N., Moeller, S., Wang, C., Ann, D., and Lee, P. P. (2015) Modulation of P2X4/P2X7/Pannexin-1 sensitivity to extracellular ATP via ivermectin induces a non-apoptotic and inflammatory form of cancer cell death. *Sci. Rep.* **5,** 16222 CrossRef Medline
30. Xie, Y., Hou, W., Song, X., Yu, Y., Huang, J., Sun, X., Kang, R., and Tang, D. (2016) Ferroptosis: process and function. *Cell Death Differ.* **23,** 369–379 CrossRef Medline
31. Cheloni, G., and Slaveykova, V. I. (2013) Optimization of the C11-BODIPY(581/591) dye for the determination of lipid oxidation in *Chlamydomonas reinhardtii* by flow cytometry. *Cytometry A* **83,** 952–961 CrossRef Medline
32. Mancias, J. D., Wang, X., Gygi, S. P., Harper, J. W., and Kimmelman, A. C. (2014) Quantitative proteomics identifies NCOA4 as the cargo receptor mediating ferritinophagy. *Nature* **509,** 105–109 CrossRef Medline
33. Ward, D. M., and Kaplan, J. (2012) Ferroportin-mediated iron transport: expression and regulation. *Biochim. Biophys. Acta* **1823,** 1426–1433 CrossRef Medline
34. Mancias, J. D., Pontano Vaites, L., Nissim, S., Biancur, D. E., Kim, A. J., Wang, X., Liu, Y., Goessling, W., Kimmelman, A. C., and Harper, J. W. (2015) Ferritinophagy via NCOA4 is required for erythropoiesis and is regulated by iron dependent HERC2-mediated proteolysis. *Elife* 10.7554/eLife.10308 CrossRef Medline
35. Visarius, T. M., Putt, D. A., Schare, J. M., Pegouske, D. M., and Lash, L. H. (1996) Pathways of glutathione metabolism and transport in isolated proximal tubular cells from rat kidney. *Biochem. Pharmacol.* **52,** 259–272 CrossRef Medline
36. Zager, R. A., Burkhart, K. M., Conrad, D. S., and Gmur, D. J. (1995) Iron, heme oxygenase, and glutathione: effects on myohemoglobinuric proximal tubular injury. *Kidney Int.* **48,** 1624–1634 CrossRef Medline
37. Banjac, A., Perisic, T., Sato, H., Seiler, A., Bannai, S., Weiss, N., Kölle, P., Tschoep, K., Issels, R. D., Daniel, P. T., Conrad, M., and Bornkamm, G. W. (2008) The cystine/cysteine cycle: a redox cycle regulating susceptibility *versus* resistance to cell death. *Oncogene* **27,** 1618–1628 CrossRef Medline
38. Ishii, T., Bannai, S., and Sugita, Y. (1981) Mechanism of growth stimulation of L1210 cells by 2-mercaptoethanol *in vitro*: role of the mixed disulfide of 2-mercaptoethanol and cysteine. *J. Biol. Chem.* **256,** 12387–12392 Medline
39. Nissen, J. D., Lykke, K., Bryk, J., Stridh, M. H., Zaganas, I., Skytt, D. M., Schousboe, A., Bak, L. K., Enard, W., Pääbo, S., and Waagepetersen, H. S. (2017) Expression of the human isoform of glutamate dehydrogenase, hGDH2, augments TCA cycle capacity and oxidative metabolism of glutamate during glucose deprivation in astrocytes. *Glia* **65,** 474–488 CrossRef Medline
40. Ribas, V., García-Ruiz, C., and Fernández-Checa, J. C. (2014) Glutathione and mitochondria. *Front. Pharmacol.* **5,** 151 Medline
41. Sun, X., Ou, Z., Chen, R., Niu, X., Chen, D., Kang, R., and Tang, D. (2016) Activation of the p62-Keap1-NRF2 pathway protects against ferroptosis in hepatocellular carcinoma cells. *Hepatology* **63,** 173–184 CrossRef Medline
42. Bauckman, K. A., and Mysorekar, I. U. (2016) Ferritinophagy drives uropathogenic *Escherichia coli* persistence in bladder epithelial cells. *Autophagy* **12,** 850–863 CrossRef Medline
43. Lin, L., Huang, S., Zhu, Z., Han, J., Wang, Z., Huang, W., and Huang, Z. (2018) P2X7 receptor regulates EMMPRIN and MMP9 expression through AMPK/MAPK signaling in PMA-induced macrophages. *Mol. Med. Rep.* **18,** 3027–3033 Medline
44. Prus, E., and Fibach, E. (2008) Flow cytometry measurement of the labile iron pool in human hematopoietic cells. *Cytometry A* **73,** 22–27 CrossRef Medline
45. Li, Y. M., Zhang, J., Su, L. J., Kellum, J. A., and Peng, Z. Y. (2019) Down-regulation of TIMP2 attenuates sepsis-induced AKI through the NF-κb pathway. *Biochim. Biophys. Acta Mol. Basis Dis.* **1865,** 558–569 CrossRef Medline
46. Chen, D., Eyupoglu, I. Y., and Savaskan, N. (2017) Ferroptosis and Cell Death Analysis by Flow Cytometry. *Methods Mol Biol.* **1601,** 71–77 CrossRef Medline